
Inductive-bias-driven Reinforcement Learning for Efficient Schedules in Heterogeneous Clusters

Subho S. Banerjee¹ Saurabh Jha¹ Zbigniew T. Kalbarczyk¹ Ravishankar K. Iyer¹

Abstract

The problem of scheduling of workloads onto heterogeneous processors (e.g., CPUs, GPUs, FPGAs) is of fundamental importance in modern data centers. Current system schedulers rely on application/system-specific heuristics that have to be built on a case-by-case basis. Recent work has demonstrated ML techniques for automating the heuristic search by using black-box approaches which require significant training data and time, which make them challenging to use in practice. This paper presents Symphony, a scheduling framework that addresses the challenge in two ways: (i) a domain-driven Bayesian reinforcement learning (RL) model for scheduling, which inherently models the resource dependencies identified from the system architecture; and (ii) a sampling-based technique to compute the gradients of a Bayesian model without performing full probabilistic inference. Together, these techniques reduce both the amount of training data and the time required to produce scheduling policies that significantly outperform black-box approaches by up to 2.2 \times .

1. Introduction

The problem of scheduling of workloads on heterogeneous processing fabrics (i.e., accelerated datacenters including GPUs, FPGAs, and ASICs, e.g., Asanović (2014); Shao & Brooks (2015)), is at its core an intractable NP-hard problem (Mastrolilli & Svensson, 2008; 2009). System schedulers generally rely on application- and system-specific heuristics with extensive domain-expert-driven tuning of scheduling policies (e.g., Isard et al. (2009); Giceva et al. (2014); Lyerly et al. (2018); Mars et al. (2011); Mars & Tang (2013); Ousterhout et al. (2013); Xu et al. (2018); Yang et al. (2013); Zhang et al. (2014); Zhuravlev et al. (2010); Za-

haria et al. (2010)). Such heuristics are difficult to generate, as variations across applications and system configurations mean that significant amounts of time and money must be spent in painstaking heuristic searches. Recent work has demonstrated machine learning (ML) techniques (Delimitrou & Kozyrakis, 2013; 2014; Mao et al., 2016; 2018) for automating heuristic searches by using black-box approaches which require significant training data and time, making them challenging to use in practice.

This paper presents Symphony, a scheduling framework that addresses the challenge in two ways: (i) we use a domain-guided Bayesian-model-based partially observable Markov decision process (POMDP) (Astrom, 1965; Kaelbling et al., 1998) to decrease the amount of training data (i.e., sampled trajectories); and (ii) a sampling-based technique that allows one to compute the gradients of a Bayesian model without performing full probabilistic inference. We thus, significantly reduce the costs of (i) running a large heterogeneous computing system that uses an efficient scheduling policy; and (ii) training the policy itself.

Reducing Training Data. State-of-the-art methods for choosing an optimal action in POMDPs rely on training of neural networks (NNs) (Mnih et al., 2016; Dhariwal et al., 2017). As these approaches are model-free, training of the NN requires large quantities of data and time to compute meaningful policies. In contrast, we provide an inductive bias for the reinforcement learning (RL) agent by encoding domain knowledge as a Bayesian model that can infer the latent state from observations, while at the same time leveraging the scalability of deep learning methods through end-to-end gradient descent. In the case of scheduling, our inductive bias is a set of statistical relationships between measurements from microarchitectural monitors (Dreyer & Alpert, 1997). To the best of our knowledge, this is the first paper to exploit those relationships and measurements to infer resource utilization in the system (i.e., latent state) to build RL-based scheduling policies.

Reducing Training Time. The addition of the inductive bias, while making the training process less data-hungry (i.e., requiring fewer workload executions to train the model), comes at the cost of additional training time: the cost of performing full-Bayesian inference at every training step (Dagum & Luby, 1993; Russell et al., 1995; Binder

¹University of Illinois at Urbana-Champaign, USA. Correspondence to: Subho S. Banerjee <ssbaner2@illinois.edu>.

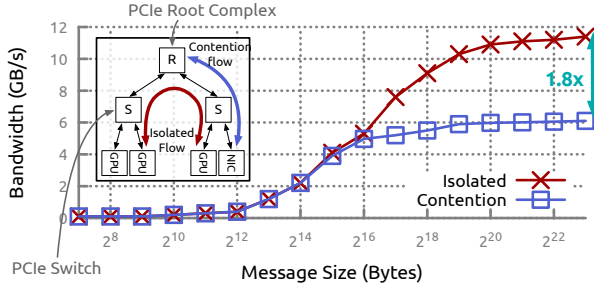


Figure 1. Performance degradation due to PCIe contention between GPU and NIC (averaged over 10 runs).

et al., 1997). It is this cost that makes the use of deep RL techniques in dynamic real-world deployments (which require periodic retraining) prohibitively expensive. To address that issue, we have developed a procedure for computing the gradient of variables in the above Bayesian model without requiring full inference computation, unlike prior work (Russell et al., 1995; Binder et al., 1997). The key is to calculate the gradient by generating samples from the model, which is computationally simpler than inferring the posterior distribution.

Need for New Scheduler. Current schedulers prioritize the use of simple generalized heuristics and coarse-grained resource bucketing (e.g., core counts, free memory) to make scheduling decisions. Hence, even though they are perceived to perform well in practice, they do not model complex emergent heterogeneous compute platforms and hence leave a lot to be desired. Consider the case of a distributed data processing framework that uses two GPUs to perform a *halo exchange*.¹ Fig. 1 shows the performance (here, bandwidth) of the exchange as “isolated” performance. If the application were to concurrently perform distributed network communication, we would observe that the original GPU-to-GPU communication is affected because of PCIe bandwidth contention at shared links (i.e., a “hidden” resource that is not often exposed to the user). Such behavior is shown as “contention” in Fig. 1, and can cause as much as a 0 – 1.8 \times slowdown, depending on the size of the transmitted messages. Traditional approaches would either have such a heuristic manually searched and incorporated into a scheduling policy, or would expect it to be found automatically as part of the training of a black-box ML model, and both approaches can require significant effort in profiling/training. In contrast, our approach allows the utilization of architectural resources (in this case, of the PCIe network) as an inductive bias for the RL-agent, thereby allowing the training process to automatically hone in on such resources of interest, without having to identify the resource’s importance manually.

Results. The Symphony framework reduces the average

¹A *halo exchange* occurs due to communication arising between parallel processors computing an overlapping pieces of data, called *halo regions*, that need to be periodically updated.

job completion time over hand-tuned scheduling heuristics by as much as 32%, and to within 6% of the time taken by an oracle scheduler. It also achieves a training time improvement of 4 \times compared to full Bayesian inference based on belief propagation. Further, the technique outperforms black-box ML techniques by 2.2 \times in terms of training time. We believe that Symphony is also representative of RL applied to several other control-related problems (e.g., industrial scheduling, data center network scheduling) where data-driven approaches can be augmented with domain knowledge to build sample-efficient RL-agents.

2. Background

Partially Observable Markov Decision Processes. A POMDP is a stochastic model that describe relationships between an agent and its environment. It is a tuple $(\mathcal{S}, \mathcal{A}, \mathcal{T}, \Omega, O, R, \gamma)$, where \mathcal{S} is the state space, \mathcal{A} is the action space, and Ω is the observation space. We use $s_t \in \mathcal{S}$ to denote the hidden state at time t . When an action $a_t \in \mathcal{A}$ is executed, the state changes according to the transition distribution, $s_{t+1} \sim \mathcal{T}(s_{t+1}|s_t, a_t)$. Subsequently, the agent receives a noisy or partially occluded observation $o_{t+1} \in \Omega$ according to the distribution $o_{t+1} \sim O(o_{t+1}|s_{t+1}, a_t)$, and a reward $r_{t+1} \in \mathbb{R}$ according to the distribution $r_{t+1} \sim R(r_{t+1}|s_{t+1}, a_t)$.

An agent acts according to its policy $\pi(a_t|s_t)$, which returns the probability of taking action a_t at time t . The agent’s goal is to learn a policy π that maximizes the expected future reward $J = \mathbb{E}_{\tau \sim p(\tau)} [\sum_{t=1}^T \gamma^{t-1} r_t]$ over trajectories $\tau = (s_0, a_0, \dots, a_{T-1}, s_T)$ induced by its policy, where $\gamma \in [0, 1)$ is the discount factor. In general, a POMDP agent must infer the belief state $b_t = \Pr(s_t|o_1, \dots, o_t, a_0, \dots, a_{t-1})$, which is used to calculate $\pi(a_t|\hat{s}_t)$ where $\hat{s}_t \sim b_t$. In the remainder of the paper, we will use $\pi(a_t|\hat{s}_t)$ and $\pi(a_t|b_t)$ interchangeably.

Related Work. Finding solutions for many POMDPs involves (i) estimating the transition model T and observation model O , (ii) performing inference under this model, and (iii) choosing an action based on the inferred belief state. Prior work in this area has extensively explored the use of NNs, particularly recurrent NNs (RNNs), as universal function approximators for (i) and (iii) above because they can be easily trained and have efficient inference procedures (e.g., Hausknecht & Stone (2015); Narasimhan et al. (2015); Mnih et al. (2015); Jaderberg et al. (2016); Foerster et al. (2016); Karkus et al. (2017); Zhu et al. (2018)). Neural networks have proven to be extremely effective at learning, but usually require a lot of data (for RL-agents, sampled trajectories, which may be prohibitively expensive to acquire for certain classes of applications, such as scheduling). The ability to incorporate explicit domain knowledge (which in the case of scheduling, is based on system design invariants) could significantly reduce the amount of data required. To

that end, other work (Karkus et al., 2017; Silver et al., 2017; Igl et al., 2018) has advocated the integration of probabilistic models (including Bayesian filter models) for (i) above. The significant computational cost of learning and inference in such deep probabilistic models has spurred the use of approximation techniques for training and inference, including NN-based approximations of Bayesian inference (Karkus et al., 2017; Zhu et al., 2018) and variational inference methods (Igl et al., 2018).

In this paper, we too advocate the use of a domain-driven probabilistic model for b_t that can be trained through end-to-end back-propagation to compute a policy. Specifically, the technique handles the gradient descent procedure on a Bayesian network (BN) with known structure and incomplete observations without performing inference on the BN, only requiring generation of samples from the model. That approach is different from prior work on learning BNs using gradient descent (Russell et al., 1995; Binder et al., 1997) or expectation maximization, both of which require full posterior inference at every training step.

Actor-Critic Methods. Actor-Critic methods (Konda & Tsitsiklis, 2000) have previously been proposed for learning the parameters ρ of an agent’s policy $\pi_\rho(a_t|s_t)$. Here (i) the “Critic” estimates the value function $V(s)$, and (ii) the “Actor” updates the policy $\pi(a|s)$ in the direction suggested by the Critic. In this paper, we use n -step learning with the asynchronous advantage actor-critic (A3C) method (Mnih et al., 2016). For n -step learning, starting at time t , the current policy performs n_s consecutive steps in n_e parallel environments. The gradient updates of π and V are based on that mini-batch of size $n_e n_s$. The target for the value function $V_\eta(s_{t+i})$, $i \in [0, n_s)$, parameterized by η , is the discounted sum of on-policy rewards up until $t + n_s$ and the off-policy bootstrapped value $V_\eta^*(s_{t+n_s})$. If we use an advantage function $A_\eta^{t,i} = (\sum_{j=0}^{n_s-i-1} \gamma^j r_{t+i+j}) + \gamma^{n_s-i} V_\eta^*(s_{t+n_s}) - V_\eta(s_{t+i})$, the value function is

$$\mathcal{L}_t^A(\rho) = -\frac{1}{n_e n_s} \sum_{e=0}^{n_e-1} \sum_{i=0}^{n_s-1} \mathbb{E}_{s_{t+i} \sim b_{t+i}} [\log \pi_\rho(a_{t+i}|s_{t+i}) A_\eta^{t,i}(s_{t+i}, a_{t+i})] \quad (1a)$$

$$\mathcal{L}_t^V(\eta) = \frac{1}{n_e n_s} \sum_{e=0}^{n_e-1} \sum_{i=0}^{n_s-1} \mathbb{E}_{s_{t+i} \sim b_{t+i}} [A_\eta^{t,i}(s_{t+i}, a_{t+i})^2]. \quad (1b)$$

3. Training the POMDP RL-Agent with Back-Propagation

We consider a special case of the POMDP formulation presented above (illustrated in Fig. 2). We assume that the domain knowledge about the environment of the RL-agent is presented as a joint probability distribution $\Pr(s_t, a_{t-1}, o_t; \Theta_{BN})$ that can be factorized as a BN (with

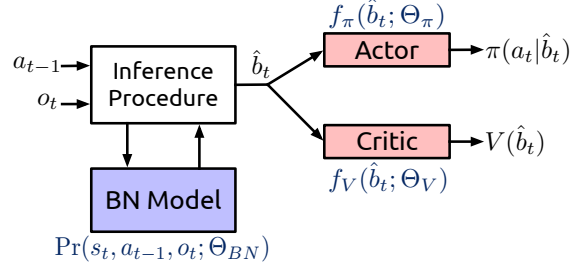


Figure 2. The proposed RL architecture.

parameters Θ_{BN}). A BN is a probabilistic graphical model that represents a set of variables and their conditional dependencies via a directed acyclic graph (DAG). We use probabilistic inference on the BN to calculate an estimate of the belief state \hat{b}_t . \hat{b}_t is then used in an NN $f_\pi(\hat{b}_t; \Theta_\pi)$ (with parameters Θ_π) to approximate the RL-agent’s policy, and an NN $f_V(\hat{b}_t; \Theta_V)$ (with parameters Θ_V) to approximate the state-based value function. We refer to all the parameters of the model as $\Theta = (\Theta_{BN}, \Theta_\pi, \Theta_V) = (\rho, \eta)$. The model is then trained by propagating the gradient of the total loss $\nabla_{\Theta} \mathcal{L}_t^{RL} = \nabla_{\Theta} \mathcal{L}_t^A(\rho) + \nabla_{\Theta} \mathcal{L}_t^V(\eta)$. Estimating this gradient requires us to compute $\nabla_{\Theta_{BN}} \hat{b}_t$. Traditional methods for computing the gradient require inference computation (Russell et al., 1995; Binder et al., 1997). However, even approximate inference in such models is known to be NP-Hard (Dagum & Luby, 1993). Below we describe an algorithm for approximating the gradient without requiring computation of full Bayesian inference. All that is required is the ability to generate samples from the BN. Only the subset of the BN necessary for generation of the samples is expanded. The samples are then used as a representation of the distribution of the BN. As a result, the proposed method decouples the training of the BN from the inference procedure used on it to calculate \hat{b}_t .

3.1. The Bayesian Network & Its Gradient

Let the BN described above be a DAG (V, E) , and let $\mathbf{X} = \{X_v | v \in V\}$ be a set of random variables indexed by V . Associated with each node X is a conditional probability density function $\Pr(X|\varphi(X))$, where $\varphi(X)$ are the parents of X in the graph. We assume that we are given (i) an efficient algorithm for sampling values of X given $\varphi(X)$, and (ii) a function $f_X(x, y; \theta_X) = \Pr_{\theta_X}(X = x | \varphi(X) = y)$ whose partial derivative with respect to θ_X is known and efficiently computable. The BN can also have deterministic relationships between two random variables, under the assumption that the relationship is a differentiable diffeomorphism. That is, for random variables X, Y , and diffeomorphism F , $\Pr(Y = y) = \Pr(X = F^{-1}(y)) | DF^{-1}(y) |$ where DF^{-1} is the inverse of the Jacobian of F .

Computing Gradient. For a random variable X in the BN, we define its parents as $\varphi(X)$, its ancestor set as $\Xi(X) = \{Y | Y \rightsquigarrow X \wedge Y \notin \varphi(X)\}$ (where \rightsquigarrow repre-

sents a directed path in the BN). We now define a procedure to approximately compute the gradient of X with respect to Θ_{BN} . We do so in two parts: (i) $\frac{\partial \Pr(X=x|\xi=\mathbf{a})}{\partial \theta_X}$ and (ii) $\nabla_{\Theta_{BN} \setminus \theta_X} \Pr(X=x|\xi=\mathbf{a})$ for $\xi \subseteq \Xi(X)$. First,

$$\begin{aligned} & \frac{\partial \Pr(X=x|\xi=\mathbf{a})}{\partial \theta_X} \\ &= \frac{\partial}{\partial \theta_X} \int \Pr(\varphi(X)=\mathbf{y}|\xi=\mathbf{a}) \times \\ & \quad \Pr(X=x|\varphi(X)=\mathbf{y}, \xi=\mathbf{a}) d\mathbf{y} \\ &= \frac{\partial}{\partial \theta_X} \int \Pr(\varphi(X)=\mathbf{y}|\xi=\mathbf{a}) f_X(x, \mathbf{y}; \theta_X) d\mathbf{y} \\ &= \int \Pr(\varphi(X)=\mathbf{y}|\xi=\mathbf{a}) \frac{\partial f_X(x, \mathbf{y}; \theta_X)}{\partial \theta_X} d\mathbf{y} \\ &\approx \sum_{i=1}^S \frac{n_S(\mathbf{a}, \mathbf{y}_i)}{n_S(\mathbf{a})} \frac{\partial f_X(x, \mathbf{y}_i; \theta_X)}{\partial \theta_X}. \end{aligned} \quad (2)$$

Here, S samples are drawn from a variable(s) Z such that $n_S(j)$ is the number of times the value j appears in the set of samples $\{z_i\}$, i.e., $n_S(j) = \sum_{i=1}^S \mathbb{1}\{z_i = j\}$. Next,

$$\begin{aligned} & \nabla_{\Theta_{BN} \setminus \theta_X} \Pr(X=x|\xi=\mathbf{a}) \\ &= \nabla_{\Theta_{BN} \setminus \theta_X} \int \Pr(\varphi(X)=\mathbf{y}|\xi=\mathbf{a}) \times \\ & \quad \Pr(X=x|\varphi(X)=\mathbf{y}, \xi=\mathbf{a}) d\mathbf{y} \\ &= \int f_X(x, \mathbf{y}; \theta_X) \nabla_{\Theta_{BN} \setminus \theta_X} \Pr(\varphi(X)=\mathbf{y}|\xi=\mathbf{a}) d\mathbf{y} \\ &\approx \sum_{i=1}^S \frac{n_S(\mathbf{y}_i)}{S} f_X(x, \mathbf{y}_i; \theta_X) \nabla_{\Theta_{BN} \setminus \theta_X} \Pr(\varphi(X)=\mathbf{y}_i|\xi=\mathbf{a}) \end{aligned} \quad (3)$$

When $|\varphi(X)| > 1$, variables in $\varphi(X)$ might not be conditionally independent given $\Xi(X)$. Hence we find a set of nodes N such that $I \perp J | \Xi(X) \cup N \forall I, J \in \varphi(X)$. Then,

$$\begin{aligned} & \Pr(\varphi(X)=\mathbf{y}_i|\xi=\mathbf{a}) \\ &= \int \Pr(N=\mathbf{n}|\xi=\mathbf{a}) \Pr(\varphi(X)=\mathbf{y}|N=\mathbf{n}, \xi=\mathbf{a}) d\mathbf{n} \\ &= \int \Pr(N=\mathbf{n}|\xi=\mathbf{a}) \prod_{j=1}^m \Pr(P_j=y_j|N=\mathbf{n}, \xi=\mathbf{a}) d\mathbf{n} \\ &\approx \sum_{k=1}^S \frac{n_S(\mathbf{a}, \mathbf{n}_k)}{n_S(\mathbf{a})} \prod_{j=1}^m \Pr(P_j=y_j|N=\mathbf{n}_k, \xi=\mathbf{a}), \end{aligned} \quad (4)$$

where $\varphi(X) = (P_1, \dots, P_m)$ and $\mathbf{y}_i = (y_{i,1}, \dots, y_{i,m})$. Thus, we obtain,

$$\begin{aligned} & \nabla_{\Theta_{BN} \setminus \theta_X} \Pr(\varphi(X)=\mathbf{y}_i|\xi=\mathbf{a}) \\ &\approx \sum_{k=1}^S \frac{n_S(\mathbf{a}, \mathbf{n}_k)}{n_S(\mathbf{a})} \times \end{aligned}$$

$$\begin{aligned} & \nabla_{\Theta_{BN} \setminus \theta_X} \prod_{j=1}^m \Pr(P_j=y_{i,j}|N=\mathbf{n}_k, \xi=\mathbf{a}) \\ &= \sum_{k=1}^S \frac{n_S(\mathbf{a}, \mathbf{n}_k)}{n_S(\mathbf{a})} \times \\ & \quad \sum_{l=1}^m \left(\prod_{h=1, h \neq l}^m \Pr(P_h=y_{i,h}|N=\mathbf{n}_k, \xi=\mathbf{a}) \right) \times \\ & \quad \nabla_{\Theta_{BN} \setminus \theta_X} \Pr(P_l=y_{i,l}|N=\mathbf{n}_k, \xi=\mathbf{a}) \\ &\approx \sum_{k=1}^S \frac{n_S(\mathbf{a}, \mathbf{n}_k)}{n_S(\mathbf{a})} \sum_{l=1}^m \left(\prod_{h=1, h \neq l}^m \frac{n_S(y_{i,h}, a, \mathbf{n}_k)}{n_S(a, \mathbf{n}_k)} \right) \times \\ & \quad \underbrace{\nabla_{\Theta_{BN} \setminus \theta_X} \Pr(P_l=y_{i,l}|N=\mathbf{n}_k, \xi=\mathbf{a})}_{\text{Expand by recursion using Eqns. 2, 3, and 5}}. \end{aligned} \quad (5)$$

The term $\nabla_{\Theta_{BN} \setminus \theta_X} \Pr(P_l=y_{i,l}|N=\mathbf{n}_k, \xi=\mathbf{a})$ represents the gradient operator on a subset of the original BN, containing only the ancestors (from the BN's graphical structure) of X . Hence that gradient term can be recursively expanded using Eqns. 2, 3, and 5. Repeating that process for all variables in \hat{b}_t allows us to calculate the $\nabla_{\Theta_{BN}} \hat{b}_t$.

Computational Complexity. The cost of computing Eqns. 2, and 3 is $O(S)$. The cost of computing Eqn. 5 is $O(mS)$. The cost of finding N is $O(|\varphi(s_t)|^2(|V|+|E|))$ (i.e., the cost of running the Bayes ball algorithm (Shachter, 2013) for every pair of nodes in $\varphi(X)$). The total computational complexity of the entire procedure hinges on finding the number of times Eqns. 2, 4, and 5 are executed, which we refer to as Q . Q depends on the size of N and on the graphical structure of the BN. Hence, the total cost of computing $\nabla_{\Theta_{BN}} \hat{b}_t$ is $O(Q(|\varphi(s_t)|^2(|V|+|E|)+mS))$ (where $|\varphi(s_t)| \leq |V|-1$, which is computed $n_s n_e |b_t|$ times during training. Note that for a polytree BN (the graphical structure of the BN we will use in §4), $N = \emptyset$, and $Q \leq |V|$. This is still better than belief propagation on the polytree with the gradient computation technique from Russell et al. (1995); Binder et al. (1997), which is $O(|V| \max_{v \in V} (dom(X_v)))$, where $dom(X)$ is the size of the domain of X , which could be exponentially large.

4. Scheduling Data Center Workloads By Using Reinforcement Learning

We now demonstrate an application of the POMDP model and training methodology presented in §3 to the problem of scheduling tasks on a heterogeneous processing fabric that includes CPUs, GPUs, and FPGAs. The model integrates real-time performance measurements, prior knowledge about workloads, and system architecture to (i) dynamically infer system state (i.e., resource utilization), and (ii) automatically schedule tasks on a heterogeneous processing fabric.

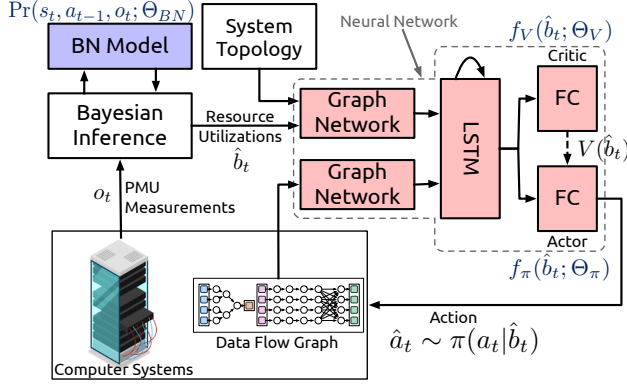


Figure 3. Architecture of the Symphony ML model.

Workload & Programming Model. The system workload consists of multiple user programs, and each program is expressed as a *data flow graph* (DFG). A DFG is a DAG where the nodes represent computations (which we refer to as *kernels*, e.g., matrix multiplication), and edges represent input-output relationships between the nodes. Prior work has shown that a large number of applications can be expressed as compositions of such kernels (Asanović et al., 2009; Banerjee et al., 2016). Prominent examples of such compositions include modern data analytics and ML frameworks that describe workloads as DFGs (Abadi et al., 2016; Chambers et al., 2010; McCool et al., 2012; Zaharia et al., 2012). We assume that the kernels are known ahead of time and have multiple implementations available for different processors and accelerators. That assumption is correct for many ML workloads; for other workloads, it is an area of active research wherein accelerator designers and architects are trying to decompose larger applications into smaller pieces. Once trained, our approach can schedule any composition (DFG) of the kernels, but requires retraining when the set of available kernels change.

POMDP Architecture. The overall architecture of the Symphony POMDP model is illustrated in Fig. 3. The first part of the POMDP models the latent state \hat{b}_t of the computer system. For the scheduling problem, \hat{b}_t corresponds to resource utilization of various components of the computer system. Utilization of some of the resources can be measured directly in software (e.g., the amount of free memory); however, the different layers of abstraction of the computer stack hide some others from direct measurement. For example, consider the example in Fig. 1 in §1; here, PCIe link bandwidth cannot be directly measured. However, it can be measured indirectly by using the number of outstanding requests to memory from each PCIe device and by using the topology of the PCIe network. In essence, we statistically relate the back pressure of one resource on another, until we can find a resource that can be directly measured via real-time performance counter (PC) measurements (o_t) (Dreyer & Alpert, 1997). We refer to such resources whose utilization cannot be directly measured as *hidden* resources.

PCs are special-purpose registers present in the CPU and other accelerators for characterization of an application’s behavior and identification of microarchitectural performance bottlenecks. Specifically, we use a BN to (i) model aleatoric uncertainty in measurements, and (ii) encode our knowledge about system architecture in terms of invariants or statistical relationships between the measurements. Inference on that BN then gives us an accurate estimate of the latent state of the system. Second, we use an RNN (i.e., $f_\pi(\cdot)$ and $f_V(\cdot)$) to learn scheduling policies for user programs that minimize resource contention and maximize performance. Those two ML models effectively decouple system-architecture-specific and measurement-specific aspects of scheduling (the BN) from its optimization aspects (the NN). The compelling value of the above architecture (and its two constituent models) is that it can automatically generate scheduling policies for the deployment of DFGs in truly heterogeneous environments (that have CPUs, GPUs, and FPGAs) without requiring configuration specifics, or painstakingly tuned heuristics. The model improves overall performance and resource utilization, and enables fine-grained resource sharing across workloads.

Performance Counters. PCs are generally relied upon to conduct low-level performance analysis or tuning of performance bottlenecks in applications. As the source of such bottlenecks is generally the unavailability of system resources, the performance counter can naturally be used to estimate resource utilization of a system. Another benefit of using PCs is that it is not necessary to modify an application’s source code in order to make measurements. PCs can be grouped into three categories: (i) those pertaining to the processing fabric (CPU core or accelerators); (ii) those pertaining to the memory subsystem; and (iii) those pertaining to the system interconnect (in our case, PCIe). Fig. 4 illustrates the organization of a computer system as well as the categories above. Fig. 5 shows a mapping between the system organization and the PCs that are used in the BN model (described below).²

BN Model. Measurements made from PCs have some inherent noise (Weaver & McKee, 2008). The measurements can only be stored in a fixed number of registers. Hence, only a fixed number of measurements can be made at any one point in time. As a result, one must make successive measurements that capture marginally different system states. Particular performance counters might become unavailable (or return incorrect values). Finally, if a single scheduling agent is controlling a cluster of machines (which is common in data centers), measurements made on different machines will not be in sync and will often be delayed by network latency. As a result, PCs are often sampled N times between successive scheduler invocations to get around some of the sources of error. To maximize the per-

²A complete list of the PCs used in this paper can be found in the supplementary material.

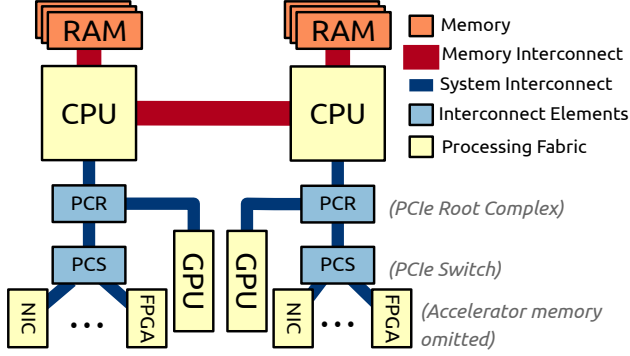


Figure 4. Organization of a multi-CPU computer.

performance estimation fidelity, we apply statistical methods to systematically model the variance of the measurements. For a single performance counter $o_t[c]$, if the error in measurement e_c can be modeled, then the measured value m_c can be modeled in terms of the true value v_c plus measurement noise e_c , i.e., $m_c = v_c + e_c$. Here, we focus only on random errors, and assume zero systematic error. That is a valid assumption because the only reason for systematic errors is hardware or software bugs. We assume that the error can be modeled as $e_c \sim \mathcal{N}(0, \sigma)$ for some unknown variance σ ; hence, $\Pr(m_c | v_c) = \mathcal{N}(m_c, \sigma)$. That follows from prior work based on extensive measurement studies (Weaver & McKee, 2008). Now, given N measurements of the value of the performance counter, we compute their sample mean μ and sample variance S . A scaled and shifted t-distribution describes the marginal distribution of the unknown mean of a Gaussian, when the dependence on variance has been marginalized out (Gelman et al., 1995); i.e., $v_c \sim \mu + S/\sqrt{N} \text{ Student}(\nu = N - 1)$. In our experiments, the confidence level of the t-distribution was 95%.

Now, given a distribution of v_c for every element of o_t , we describe the construction of the BN model. Our goal is to model resource utilization (a number in $[0, 1]$) for a relevant set of architectural resources R . To do so, we use algebraic models for composing PC measurements (v_c) by using algebraic (deterministic) relationships derived from information about the CPU architecture. Processor performance manuals (Yasin, 2014; Intel Corp., 2016; Hall et al., 2017) and or vendor contributions in OS codebases (e.g., in the `perf` module in Linux) provide such information. When available in the later format (which is indeed the case for all modern Intel, AMD, ARM, and IBM CPUs), these relationships can be automatically parsed and be used to construct the BN.

As our error-corrected measurements are defined in terms of distributions, the algebraic models that encode static information about relationships (based on the microarchitecture of the processor or topology of the system) now define statistical relationships v_c s (based on the Jacobian relationships described in §3). Fig. 5 shows an example of the BN model. However, the types and meanings of hardware counters vary from one kind of architecture to another because of

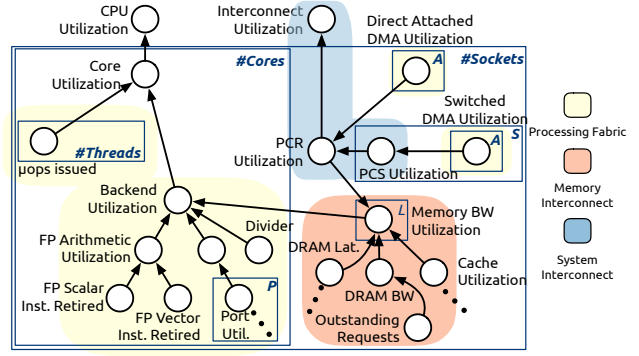


Figure 5. Bayesian network (uses the plate notation) used to estimate resource utilization.

the variation in hardware organizations. As a result, the model defined by the BN is parametric, changing with different processors and system topologies (i.e., across all the different types of systems in a data center).

Consider the example of identifying memory bandwidth utilization for a CPU core. According to the processor documentation, the utilization can be computed by measuring the number of outstanding memory requests (which is available as a PC), i.e., $\text{Outstanding Requests}[\geq \theta_{MB}] / \text{Outstanding Requests}[\geq 1]$.³ That is, identify the fraction of cycles in some time window that CPU-core stalls because of insufficient bandwidth. Naturally, in order to sustain maximum performance, it is necessary to ensure that no stalls occur. The value θ_{MB} is processor-specific and might not always be known. In such cases, we use the training approach described in §3 to learn θ_{MB} . The procedure is repeated for all relevant system utilization counters (marked as “Util.” in Fig. 5), which together represent \hat{b}_t . Such a BN model for a 16-core Intel Xeon processor (with all PCIe lanes populated) has 68 nodes, of which 32 are directly measured and the remainder are computed through inference.

BN Retraining. The architectural information required to build the BN can be found in processor manuals (Intel Corp., 2016; Sudhakar & Srinivasan, 2019; Hall et al., 2017) as well as in machine-parsable databases in the Linux kernel source code as part of the `perf` package. The only human intervention required in the process of building the BN is for filtering out those resources that cannot be controlled with software (because they change too quickly). The BN model should only be rebuilt when the underlying hardware configuration changes, which Mars & Tang (2013) observe happens every 5–6 years in a data center.

Implementation Details. We collect system-wide (for all processes) performance counter measurements for a variety of hardware events (described in Table 1). The system wide collection leads to occasional spurious measurements (e.g., from interrupt handlers), however, this allows us to make holistic measurements (e.g., capture system calls or

³Here $X[\geq t]$ counts cycles in which X exceeds threshold t .

Table 1. Performance counters used in test evaluation. We have disambiguated the names to ensure platform independence.

Performance Counters/Events
On-core Events
Core Clock Cycles, Reference Clock Cycles, Temperature, Instructions (μ ops for Intel) issued, Instructions (μ ops for Intel) retired, Un-utilized slots due to miss-speculation
Un-core & Memory Controller Events (per socket)
#Read/Write requests to DRAM (from all channels), #Local DRAM accesses, #Remote DRAM Accesses, #Read/Write requests to DRAM (from all channels) from IO sources, #PCIe Read, #PCIe Write, QPI (for Intel)/Nest (for IBM) Transactions
OS/Driver Events
Free memory (CPU, GPU, FPGA), Total memory (CPU, GPU, FPGA)

drivers that perform memory and DMA operations). We make the minimum measurements to infer if a kernel scheduled to a CPU-hardware thread is core-bound (floating point and integer-intensive). This allows us to make scheduling decisions on co-located kernels, i.e., those that get scheduled to SMT/hyperthreads bound to a core. The majority of measurements are made at the level of un-core events that captures performance of the memory interconnect and the system bus: to identify kernels that are bandwidth bottlenecked. We do not explicitly model GPU performance counters as low-level scheduling decisions (e.g., warp-level scheduling) in GPUs are obfuscated by the NVIDIA runtime/driver.

NN Model. The second part of the POMDP-based scheduling model uses an NN (see Fig. 3) to learn the optimal policy with which to schedule user tasks given a belief state. The NN takes two graphs as inputs. The first input is the belief state \hat{b}_t , encoded as vertex labels on a graph that describes the topology of a computer system (i.e., the organization shown in Fig. 4), and input labels that correspond to the locations of inputs in the topology. The color coding in Figs. 4, and 5 shows a mapping (i.e., vertex labels) between nodes in the topology graph and \hat{b}_t . The second input is the user’s program expressed as a DFG. We use *graph network* (GN) layers (Battaglia et al., 2018) to “embed” the graphs into a set of *embedding vectors*. GNs have been shown to capture node, edge, and locality information. We chose small, fully connected NNs for modeling the functional transformations in the GN layers. Prior work in scheduling (e.g., Grandl et al. (2016b); Wu et al. (2012)) has shown the benefit of considering temporal information to capture the dependencies of system resources over time as well as the time evolution of the user DFG. We capture those relationships (between the embeddings of the input graphs) by using an RNN, specifically an LSTM layer (Hochreiter &

Schmidhuber, 1997).

The action space \mathcal{A} of the model is fixed as the number of kernels/processors available in the system and is known ahead of time. The action space consists of the following types of actions. (i) *Execution actions* correspond to execution of a kernel on a processor/accelerator. (ii) *Reconfiguration actions* correspond to reconfiguration of a single FPGA context to a kernel. (iii) *No-Op actions* correspond to not scheduling any task in a particular scheduler invocation. No-Ops are useful when the system resources are maximally subscribed, and execution of more tasks will hinder performance. The scheduler is invoked every time there is an idle processor/accelerator in the system (i.e., every time a processor finishes the work assigned to it), causing the system to take one of the above actions.

Reward Function. The reward r_t is based on the objective of minimizing the runtime of a user DFG. At time t , $r_t = -\sum_{i=0}^t 1/T_i$, where T_i is the wall clock time taken to execute the i actions executing in the system at time t . We picked r_t as it represents the “makespan” of the schedule, a metric that is popularly used in the traditional scheduling literature and accurately represents the user-facing performance of the system. Note that parallel actions are not double-counted in this formulation. The BN and NN models are trained end-to-end using minimization of Eqn. 1 through back-propagation, as described in §3.

Implementation details of the BN and NN models are presented in the supplementary material.

5. Evaluation & Discussion

We evaluated the Symphony along the following dimensions. (i) *How well does Symphony perform compared to the state of the art?* (ii) *How does the Symphony’s runtime affect scheduling decisions?* (iii) *What are the savings in training time compared to traditional methods?* The evaluation testbed consisted of a rack-scale cluster of twelve IBM Power8 CPUs, two NVIDIA K40, six K80 GPUs, and two FPGAs. We illustrated the generality of techniques on a variety of real-world workloads that used CPUs, GPUs, and FPGAs: (i) *variant calling and genotyping analysis* (Van der Auwera et al., 2013) on human genome datasets using tools presented in Banerjee et al. (2016; 2017; 2019a); Li & Durbin (2009; 2010); Langmead et al. (2009); McKenna et al. (2010); Nothaft et al. (2015); Nothaft (2015); Rimmer et al. (2014); Zaharia et al. (2011); (ii) *epilepsy detection and localization* (Varatharajah et al., 2017) on intra-cranial electroencephalography data; and (iii) in online *security analytics* (Cao et al., 2015) for intrusion detection systems.

State of the Art. Traditional dynamic scheduling techniques (e.g., Isard et al. (2009); Giceva et al. (2014); Lysterly et al. (2018); Ousterhout et al. (2013); Zhuravlev et al. (2010); Zaharia et al. (2010)) use manually tuned heuristics

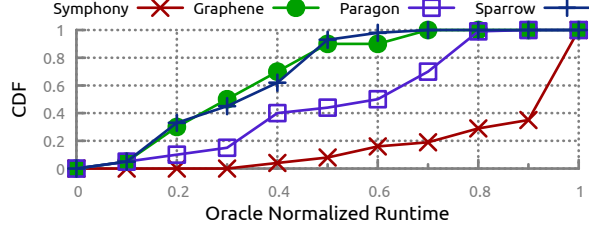


Figure 6. Comparing performance of Symphony to that of other popular schedulers for kernel executions in DFGs.

(e.g., fairness, shortest-job-first) that prioritize simplicity and generality over achieving the best-case workload performance, often allocating coarse-grained resources (e.g., GBs of memory, CPU threads) and making simplifying assumptions about the underlying workload. Several ML-based scheduling strategies have also been proposed, wherein the above heuristics are learned from data. They use a variety of black-box ML models, e.g., model-free deep RL in (Mao et al., 2016; 2018), collaborative filtering (Delimitrou & Kozyrakis, 2013; 2014), and other traditional ML techniques like SVMs (e.g., Mars et al. (2011); Mars & Tang (2013); Yang et al. (2013); Zhang et al. (2014)). A common theme in these techniques is that of treating the system as a black-box and performing scheduling to optimize application throughput metrics. The above approaches are not well-suited to heterogeneous, accelerator-rich systems in which architectural diversity necessitates the use of low-level resources, which cannot be measured directly and are not semantically comparable across processors. As points of comparison to Symphony, we used *Graphene* (Grandl et al., 2016b), a heuristic-accelerated job shop optimization solver⁴; *Sparrow* (Ousterhout et al., 2013), a randomized scheduler; and *Paragon* (Delimitrou & Kozyrakis, 2013), a collaborative filtering-based scheduler.

Baseline for Comparison. We defined the *oracle schedule* to correspond to the best performance possible for running an application on the evaluation system. It corresponds to a completely isolated execution of an application. Here, different concurrently executing kernels of the same application contend for resources and might cause performance degradation. For the benchmark applications, we accounted for that by exhaustively executing schedules of the application DFGs to find the one with the lowest runtime (i.e., the *oracle run*). We measured the runtime of kernel i in workload (in the oracle run) j as $t_{i,j}^{\text{oracle}}$ across all kernels and workloads. $t_{i,j}^{\text{oracle}}$ serves as the baseline for assessing the performance of Symphony.

Effectiveness of Scheduling Model. First, we quantified how well Symphony can handle scheduling of kernels in a DFG taking into account of resource contention and inter-

⁴Graphene was not originally designed to execute on heterogeneous systems. In the supplementary material, we explain modifications we made to the algorithm.

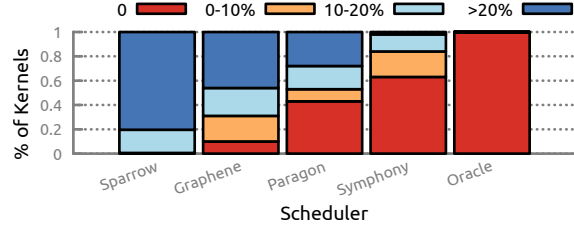


Figure 7. Percentage of application executions that show a degradation in performance.

ference at (i) intra-DFG level; and (ii) when executing with an unknown co-located workload utilizing compute and I/O resources. To do so, we measured the runtimes of each of the kernels i in the workload j (as above) to compute $t_{i,j}^s$ for each scheduler s under test. In Fig. 6, we illustrate the distribution of oracle-normalized runtimes for each of the kernels in the workloads we tested, i.e., a distribution of $t_{i,j}^s/t_{i,j}^{\text{oracle}}$ across 500 executions of the three above workloads. In the figure, a distribution whose probability mass is closest to 1 is preferred, as it implies the least slowdown compared to the oracle. We observe that the proposed technique significantly outperformed the state-of-the-art. In our experiments, the median and tail (i.e., 99th percentile) runtime of Symphony outperformed the second best (in this case, Paragon) by close to 32%. At the 99th percentile, the generated schedules performed at a 6% loss relative to the oracle. Next, we quantified the performance of end-to-end user workloads, shown in Fig. 7. Here, we calculated $1 - (\sum_i t_{i,j}^s) / (\sum_i t_{i,j}^{\text{oracle}})$ for all 500 runs of the DFGs and grouped them into buckets of different kinds of normalized performance. Symphony significantly outperformed the other scheduling techniques, running up to 60% of the applications with no performance loss relative to the oracle execution, and the rest with a performance loss of less than 20%.

Latency. There are two latencies to consider in comparing schedulers: the latency of the entire user workload (“LW”, shown in Fig. 6), and the latency of the scheduler execution (“LS”, shown in Fig. 8). In Fig. 8, we show two configurations of the Symphony scheduler: (i) “No-Opt” which uses a belief propagation-based update for the BN (and MCMC-based inference); and (ii) “All-Opt” which uses the sampling technique described in §3, accelerators⁵ to perform inference, and *task batching* (described below). LW (\geq LS) is the user-facing metric of interest. Symphony outperforms all baselines in terms of LW. In terms of median LS, the Symphony is 1.8 \times and 1.6 \times faster than Paragon and Graphene, respectively. In contrast, Sparrow, which randomly assigns tasks to processors, has 3.6 \times lower median latency than Symphony. However, the reduced LS comes at the cost of increased LW (see Fig. 6).

Batching Task Execution. A key concern with Symphony

⁵The accelerators include an NVIDIA K80 GPU for NN inference and an FPGA for BN inference using Banerjee et al. (2019b).

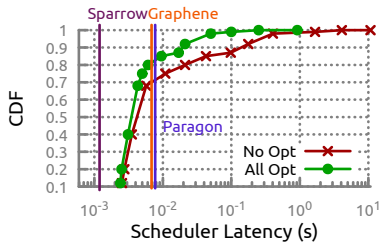


Figure 8. Symphony’s latency (“All Opt” & “No Opt”) compared to prior work.

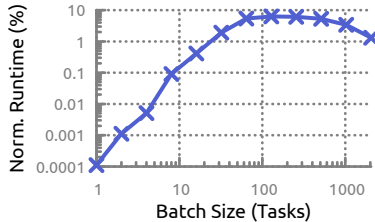


Figure 9. Symphony’s performance (oracle normalized, in %) with varying batch size.

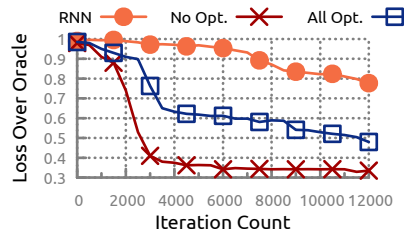


Figure 10. Training time for Symphony. An iteration is 2 RL episodes of 20 steps.

is its large tail latency (100× larger than its median; see Fig. 8) compared to the other schedulers (which have deterministic runtime). This increased latency is brought about by Symphony having to perform significantly more compute if the RL-policy-update is triggered. The scheduler latency adversely affects LW as the time spent executing scheduler calls, is time not utilized to make progress on the user workload. In order to deal with this issue, our evaluation executed Symphony on batches of tasks instead of single tasks, thereby amortizing the cost of executing Symphony across the batch. Task batching works synergistically with the sampling based gradient propagation technique to reduce the tail latency by as much 12× (see Fig. 3). Fig. 9 demonstrates the average improvement in LW normalized to the oracle over a range of batch sizes. We observe that the optimal value for batch size is about 128 tasks per batch. This corresponds to the “All Opt” configuration in Figs. 8, and 10 as well as Figs. 6, and 7. The “No Opt” configuration in Fig. 8 is computed at a batch size of one.

Training Time. Finally, we quantified the improvement in training time offered by Symphony using the sampling-based gradient computation methodology presented in §3. We used the following baselines for evaluation: (i) model-free RNN (labeled “RNN” in Fig. 10); and (ii) the “All Opt.” and “No Opt.” configurations from above. The RNN model here replaces the BN (and inference) and system-topology-embedding GN (in Fig. 3) with a 3-layer, fully connected NN to compute an embedding for o_t . Fig. 10 illustrates the differences in performance of these configurations with respect to degradation in performance of the user DFGs relative to the oracle schedule (i.e., $1 - (\sum_i t_{i,j}^s) / (\sum_i t_{i,j}^{\text{oracle}})$). We observe that the RNN is significantly less sample-efficient than the proposed POMDP is; specifically, it is $\sim 2.2\times$ worse than Symphony. Further linearly extrapolating time to convergence from iteration 12×10^3 , the RNN would need $> 48 \times 10^3$ iterations to achieve the same accuracy as Symphony.

The difference in training time for the “No Opt.” and “All Opt” in Fig. 10 can be attributed to (i) time taken to perform back-propagation for policy updates; and (ii) effective scheduler latency. Linearly extrapolating the training-loss, we observe that “All Opt” is at least 4.3× more sample efficient than “No Opt” to reach a 30% mean loss relative to the oracle. That reduction is significant because the contin-

uous churn of user workloads and machine configurations in a cloud, as pointed out in Mars et al. (2011), would require that the scheduling model be periodically retrained. In absolute terms, the “All Opt” configuration is able to achieve $\sim 30\%$ mean loss relative to the oracle scheduler in 700 hours of training and ~ 4400 iterations of workload execution. That corresponds to approximately 500 hours of system execution; hence, the total process takes 1200 hours. Though this might appear to be over 7 weeks of time, in wall clock time this is approximately 2 week because we use parallel A3C-based training. In fact, the limiting factor here is the availability of FPGAs, of which we have only 2 in the evaluation cluster, hence limiting the number of RL episodes that can be run in parallel.

6. Conclusion

This paper presents (i) a domain-driven Bayesian RL model for scheduling that captures the statistical dependencies between architectural resources; and (ii) a sampling-based technique that allows the computation of gradients of a Bayesian model without performing full probabilistic inference. As data center architectures become more complex (Asanović, 2014; Shao & Brooks, 2015), techniques like the one proposed here will be critical in the deployment of future accelerated applications.

Acknowledgments

We thank K. Saboo, S. Lumetta, W-M. Hwu, K. Atchley, and J. Applequist for their insightful comments on the early drafts of this manuscript. This research was supported in part by the National Science Foundation (NSF) under Grant Nos. CNS 13-37732 and CNS 16-24790; by IBM under a Faculty Award and through equipment donations; and by Xilinx and Intel through equipment donations. Any opinions, findings, and conclusions or recommendations expressed in this material are those of the authors and do not necessarily reflect the views of the NSF, IBM, Xilinx or Intel.

References

Abadi, M., Barham, P., Chen, J., Chen, Z., Davis, A., Dean, J., Devin, M., Ghemawat, S., Irving, G., Isard, M., Kudlur,

- M., Levenberg, J., Monga, R., Moore, S., Murray, D. G., Steiner, B., Tucker, P., Vasudevan, V., Warden, P., Wicke, M., Yu, Y., and Zheng, X. TensorFlow: A System for Large-scale Machine Learning. In *Proceedings of the 12th USENIX Conference on Operating Systems Design and Implementation*, pp. 265–283. USENIX Association, 2016.
- Asanović, K. FireBox: A Hardware Building Block for 2020 Warehouse-Scale Computers. Santa Clara, CA, February 2014. USENIX Association.
- Asanović, K., Bodik, R., Demmel, J., Keaveny, T., Keutzer, K., Kubiawicz, J., Morgan, N., Patterson, D., Sen, K., Wawrzyniec, J., Wessel, D., and Yelick, K. A View of the Parallel Computing Landscape. *Commun. ACM*, 52(10): 56–67, October 2009.
- Astrom, K. J. Optimal control of Markov processes with incomplete state information. *Journal of Mathematical Analysis and Applications*, 10(1):174–205, 1965.
- Banerjee, S. S., Athreya, A. P., Mainzer, L. S., Jongeneel, C. V., Hwu, W.-M., Kalbarczyk, Z. T., and Iyer, R. K. Efficient and scalable workflows for genomic analyses. In *Proceedings of the ACM International Workshop on Data-Intensive Distributed Computing, DIDC '16*, pp. 27–36, 2016.
- Banerjee, S. S., El-Hadedy, M., Tan, C. Y., Kalbarczyk, Z. T., Lumetta, S. S., and Iyer, R. K. On accelerating pair-HMM computations in programmable hardware. In *Proc. 27th International Conference on Field Programmable Logic and Applications, FPL 2017, Ghent, Belgium, September 4-8, 2017*, pp. 1–8, 2017.
- Banerjee, S. S., El-Hadedy, M., Lim, J. B., Kalbarczyk, Z. T., Chen, D., Lumetta, S. S., and Iyer, R. K. ASAP: Accelerated Short-Read Alignment on Programmable Hardware. *IEEE Transactions on Computers*, 68(3):331–346, March 2019a.
- Banerjee, S. S., Kalbarczyk, Z. T., and Iyer, R. K. AcMC²: Accelerating Markov Chain Monte Carlo Algorithms for Probabilistic Models. In *Proceedings of the Twenty-Fourth International Conference on Architectural Support for Programming Languages and Operating Systems*, pp. 515–528, 2019b.
- Battaglia, P. W., Hamrick, J. B., Bapst, V., Sanchez-Gonzalez, A., Zambaldi, V., Malinowski, M., Tacchetti, A., Raposo, D., Santoro, A., Faulkner, R., et al. Relational inductive biases, deep learning, and graph networks. *arXiv preprint arXiv:1806.01261*, 2018.
- Binder, J., Koller, D., Russell, S., and Kanazawa, K. Adaptive Probabilistic Networks with Hidden Variables. *Machine Learning*, 29(2/3):213–244, 1997.
- Broquedis, F., Clet-Ortega, J., Moreaud, S., Furmento, N., Goglin, B., Mercier, G., Thibault, S., and Namyst, R. hwloc: A Generic Framework for Managing Hardware Affinities in HPC Applications. In *Proc. 2010 18th EuroMicro Conference on Parallel, Distributed and Network-based Processing*, pp. 180–186, Feb 2010.
- Cao, P., Badger, E., Kalbarczyk, Z., Iyer, R., and Slagell, A. Preemptive intrusion detection: Theoretical framework and real-world measurements. In *Proceedings of the 2015 Symposium and Bootcamp on the Science of Security, HotSoS '15*, pp. 5:1–5:12, 2015.
- Chambers, C., Raniwala, A., Perry, F., Adams, S., Henry, R., Bradshaw, R., and Nathan. FlumeJava: Easy, Efficient Data-Parallel Pipelines. In *ACM SIGPLAN Conference on Programming Language Design and Implementation (PLDI)*, pp. 363–375, 2010.
- Chowdhury, M., Zhong, Y., and Stoica, I. Efficient coflow scheduling with varys. In *Proceedings of the 2014 ACM Conference on SIGCOMM, SIGCOMM '14*, pp. 443–454, 2014.
- Dagum, P. and Luby, M. Approximating probabilistic inference in Bayesian belief networks is NP-hard. *Artificial Intelligence*, 60(1):141–153, 1993.
- Delimitrou, C. and Kozyrakis, C. Paragon: QoS-aware Scheduling for Heterogeneous Datacenters. *SIGPLAN Not.*, 48(4):77–88, March 2013.
- Delimitrou, C. and Kozyrakis, C. Quasar: Resource-efficient and QoS-aware Cluster Management. In *Proceedings of the 19th International Conference on Architectural Support for Programming Languages and Operating Systems, ASPLOS '14*, pp. 127–144, 2014.
- Dhariwal, P., Hesse, C., Klimov, O., Nichol, A., Plappert, M., Radford, A., Schulman, J., Sidor, S., Wu, Y., and Zhokhov, P. OpenAI Baselines. <https://github.com/openai/baselines>, 2017.
- Doweck, J. Inside 6th generation Intel Core code named Skylake:: New Microarchitecture and Power Management. https://www.hotchips.org/wp-content/uploads/hc_archives/hc28/HC28.23-Tuesday-Epub/HC28.23.90-High-Perform-Epub/HC28.23.911-Skylake-Doweck-Intel_SK3-r13b.pdf, 2016. Accessed 2019-03-05.
- Dreyer, R. S. and Alpert, D. B. Apparatus for monitoring the performance of a microprocessor, August 1997. US Patent 5,657,253.
- Foerster, J. N., Assael, Y. M., de Freitas, N., and Whiteson, S. Learning to communicate to solve riddles with deep distributed recurrent Q-networks. *arXiv preprint arXiv:1602.02672*, 2016.

- Gelman, A., Carlin, J., Stern, H., and Rubin, D. *Bayesian Data Analysis*. Chapman & Hall, New York, 1995.
- Giceva, J., Alonso, G., Roscoe, T., and Harris, T. Deployment of query plans on multicores. *Proc. VLDB Endow.*, 8(3):233–244, November 2014.
- Grandl, R., Chowdhury, M., Akella, A., and Ananthanarayanan, G. Altruistic Scheduling in Multi-resource Clusters. In *Proceedings of the 12th USENIX Conference on Operating Systems Design and Implementation*, pp. 65–80. USENIX Association, 2016a.
- Grandl, R., Kandula, S., Rao, S., Akella, A., and Kulkarni, J. Graphene: Packing and Dependency-aware Scheduling for Data-parallel Clusters. In *Proceedings of the 12th USENIX Conference on Operating Systems Design and Implementation*, pp. 81–97, 2016b.
- Hall, B., Bergner, P., Housfater, A. S., Kandasamy, M., Magno, T., Mericas, A., Munroe, S., Oliveira, M., Schmidt, B., Schmidt, W., et al. *Performance optimization and tuning techniques for IBM Power Systems processors including IBM POWER8*. IBM Redbooks, 2017.
- Hausknecht, M. and Stone, P. Deep recurrent Q-learning for partially observable MDPs. In *2015 AAAI Fall Symposium Series*, 2015.
- Hindman, B., Konwinski, A., Zaharia, M., Ghodsi, A., Joseph, A. D., Katz, R., Shenker, S., and Stoica, I. Mesos: A platform for fine-grained resource sharing in the data center. In *Proceedings of the 8th USENIX Conference on Networked Systems Design and Implementation, NSDI' 11*, pp. 295–308. USENIX Association, 2011.
- Hochreiter, S. and Schmidhuber, J. Long short-term memory. *Neural computation*, 9(8):1735–1780, 1997.
- Igl, M., Zintgraf, L., Le, T. A., Wood, F., and Whiteson, S. Deep variational reinforcement learning for POMDPs. *arXiv preprint arXiv:1806.02426*, 2018.
- Intel Corp. Intel 64 and ia-32 architectures optimization reference manual. *Intel Corporation, Sept*, 2014.
- Intel Corp. Intel® 64 and IA-32 Architectures Software Developer Manuals. <https://software.intel.com/en-us/articles/intel-sdm>, 2016. Accessed 2019-03-05.
- Isard, M., Prabhakaran, V., Currey, J., Wieder, U., Talwar, K., and Goldberg, A. Quincy: Fair scheduling for distributed computing clusters. In *Proceedings of the ACM SIGOPS 22nd Symposium on Operating Systems Principles, SOSP '09*, pp. 261–276, 2009.
- Jaderberg, M., Mnih, V., Czarnecki, W. M., Schaul, T., Leibo, J. Z., Silver, D., and Kavukcuoglu, K. Reinforcement learning with unsupervised auxiliary tasks. *arXiv preprint arXiv:1611.05397*, 2016.
- Kaelbling, L. P., Littman, M. L., and Cassandra, A. R. Planning and acting in partially observable stochastic domains. *Artificial Intelligence*, 101(1–2):99–134, 1998.
- Karkus, P., Hsu, D., and Lee, W. S. QMDP-Net: Deep learning for planning under partial observability. In *Advances in Neural Information Processing Systems*, pp. 4694–4704, 2017.
- Kleen, A. PMU-Tools. <https://github.com/andikleen/pmu-tools>, 2010. Accessed 2019-03-05.
- Konda, V. R. and Tsitsiklis, J. N. Actor-critic algorithms. In *Advances in neural information processing systems*, pp. 1008–1014, 2000.
- Langmead, B., Trapnell, C., Pop, M., and Salzberg, S. L. Ultrafast and memory-efficient alignment of short DNA sequences to the human genome. *Genome Biol.*, 10(3):R25, 2009.
- Li, H. and Durbin, R. Fast and accurate short-read alignment with burrows-wheeler transform. *Bioinformatics*, 25(14):1754–1760, may 2009. doi: 10.1093/bioinformatics/btp324. URL <http://dx.doi.org/10.1093/bioinformatics/btp324>.
- Li, H. and Durbin, R. Fast and accurate long-read alignment with Burrows–Wheeler transform. *Bioinformatics*, 26(5):589–595, 2010.
- Li, H., Handsaker, B., Wysoker, A., Fennell, T., Ruan, J., Homer, N., Marth, G., Abecasis, G., Durbin, R., et al. The sequence alignment/map format and SAMtools. *Bioinformatics*, 25(16):2078–2079, 2009.
- Lyerly, R., Murray, A., Barbalace, A., and Ravindran, B. Aira: A framework for flexible compute kernel execution in heterogeneous platforms. *IEEE Transactions on Parallel and Distributed Systems*, 29(2):269–282, Feb 2018. ISSN 1045-9219. doi: 10.1109/TPDS.2017.2761748.
- Mao, H., Alizadeh, M., Menache, I., and Kandula, S. Resource management with deep reinforcement learning. In *Proceedings of the 15th ACM Workshop on Hot Topics in Networks*, pp. 50–56. ACM, 2016.
- Mao, H., Schwarzkopf, M., Venkatakrisnan, S. B., Meng, Z., and Alizadeh, M. Learning scheduling algorithms for data processing clusters. *arXiv preprint arXiv:1810.01963*, 2018.
- Mars, J. and Tang, L. Whare-map: Heterogeneity in "homogeneous" warehouse-scale computers. *SIGARCH Comput. Archit. News*, 41(3):619–630, June 2013.
- Mars, J., Tang, L., and Hundt, R. Heterogeneity in "homogeneous" warehouse-scale computers: A performance opportunity. *IEEE Comput. Archit. Lett.*, 10(2):29–32, July 2011. ISSN 1556-6056.

- Mastrolilli, M. and Svensson, O. (acyclic) job shops are hard to approximate. In *2008 49th Annual IEEE Symposium on Foundations of Computer Science*, pp. 583–592, Oct 2008. doi: 10.1109/FOCS.2008.36.
- Mastrolilli, M. and Svensson, O. Improved bounds for flow shop scheduling. In *International Colloquium on Automata, Languages, and Programming*, pp. 677–688. Springer, 2009.
- McCool, M., Reinders, J., and Robison, A. *Structured Parallel Programming: Patterns for Efficient Computation*. Morgan Kaufmann Publishers Inc., San Francisco, CA, USA, 1st edition, 2012. ISBN 9780123914439, 9780124159938.
- McKenna, A., Hanna, M., Banks, E., Sivachenko, A., Cibulskis, K., Kernysky, A., Garimella, K., Altshuler, D., Gabriel, S., Daly, M., and DePristo, M. A. The genome analysis toolkit: A MapReduce framework for analyzing next-generation DNA sequencing data. *Genome Research*, 20(9):1297–1303, jul 2010. doi: 10.1101/gr.107524.110.
- Mnih, V., Kavukcuoglu, K., Silver, D., Rusu, A. A., Veness, J., Bellemare, M. G., Graves, A., Riedmiller, M., Fidjeland, A. K., Ostrovski, G., et al. Human-level control through deep reinforcement learning. *Nature*, 518(7540): 529, 2015.
- Mnih, V., Badia, A. P., Mirza, M., Graves, A., Harley, T., Lillicrap, T. P., Silver, D., and Kavukcuoglu, K. Asynchronous methods for deep reinforcement learning. In *Proceedings of the 33rd International Conference on International Conference on Machine Learning - Volume 48*, ICML’16, pp. 1928–1937. JMLR.org, 2016.
- Narasimhan, K., Kulkarni, T., and Barzilay, R. Language understanding for text-based games using deep reinforcement learning. *arXiv preprint arXiv:1506.08941*, 2015.
- Nothhaft, F. Scalable genome resequencing with adam and avocado. Master’s thesis, EECS Department, University of California, Berkeley, May 2015.
- Nothhaft, F., Massie, M., Danford, T., Zhang, Z., Laseron, U., Yeksigian, C., Kottalam, J., Ahuja, A., Hammerbacher, J., Linderman, M., Franklin, M. J., Joseph, A. D., and Patterson, D. A. Rethinking data-intensive science using scalable analytics systems. In *Proceedings of the 2015 ACM SIGMOD International Conference on Management of Data*, SIGMOD ’15, pp. 631–646, New York, NY, USA, 2015. ACM. ISBN 978-1-4503-2758-9. doi: 10.1145/2723372.2742787.
- Ousterhout, K., Wendell, P., Zaharia, M., and Stoica, I. Sparrow: Distributed, low latency scheduling. In *Proceedings of the Twenty-Fourth ACM Symposium on Operating Systems Principles*, SOSP ’13, pp. 69–84, New York, NY, USA, 2013. ACM. ISBN 978-1-4503-2388-8. doi: 10.1145/2517349.2522716.
- Rimmer, A., Phan, H., Mathieson, I., Iqbal, Z., Twigg, S. R. F., Wilkie, A. O. M., McVean, G., and Lunter, G. Integrating mapping-, assembly- and haplotype-based approaches for calling variants in clinical sequencing applications. *Nature Genetics*, 46(8):912–918, jul 2014.
- Russell, S., Binder, J., Koller, D., and Kanazawa, K. Local learning in probabilistic networks with hidden variables. In *Proceedings of the 14th International Joint Conference on Artificial Intelligence - Volume 2*, IJCAI’95, pp. 1146–1152, San Francisco, CA, USA, 1995. Morgan Kaufmann Publishers Inc. ISBN 1-55860-363-8.
- Shachter, R. D. Bayes-ball: The rational pastime (for determining irrelevance and requisite information in belief networks and influence diagrams). *arXiv preprint arXiv:1301.7412*, 2013.
- Shao, Y. and Brooks, D. *Research Infrastructures for Hardware Accelerators*. Synthesis Lectures on Computer Architecture. Morgan & Claypool Publishers, 2015.
- Silver, D., van Hasselt, H., Hessel, M., Schaul, T., Guez, A., Harley, T., Dulac-Arnold, G., Reichert, D., Rabinowitz, N., Barreto, A., et al. The Predictron: End-to-end learning and planning. In *Proceedings of the 34th International Conference on Machine Learning - Volume 70*, pp. 3191–3199. JMLR, 2017.
- Stuecheli, J., Blaner, B., Johns, C. R., and Siegel, M. S. CAPI: A Coherent Accelerator Processor Interface. *IBM Journal of Research and Development*, 59(1):7:1–7:7, Jan 2015. ISSN 0018-8646. doi: 10.1147/JRD.2014.2380198.
- Sudhakar, A. T. and Srinivasan, M. IBM POWER in-memory collection counters. <https://developer.ibm.com/articles/power9-in-memory-collection-counters/>, 2019. Accessed 2019-03-05.
- Terpstra, D., Jagode, H., You, H., and Dongarra, J. Collecting Performance Data with PAPI-C. In Müller, M. S., Resch, M. M., Schulz, A., and Nagel, W. E. (eds.), *Tools for High Performance Computing 2009*, pp. 157–173, Berlin, Heidelberg, 2010. Springer Berlin Heidelberg.
- Van der Auwera, G. A., Carneiro, M. O., Hartl, C., Poplin, R., del Angel, G., Levy-Moonshine, A., Jordan, T., Shakir, K., Roazen, D., Thibault, J., Banks, E., Garimella, K. V., Altshuler, D., Gabriel, S., and DePristo, M. A. From fastq data to high-confidence variant calls: The genome analysis toolkit best practices pipeline. *Current Protocols in Bioinformatics*, 43(1):11.10.1–11.10.33, 2013.

- Varatharajah, Y., Chong, M. J., Saboo, K., Berry, B., Brinkmann, B., Worrell, G., and Iyer, R. EEG-GRAPH: A Factor-Graph-Based Model for Capturing Spatial, Temporal, and Observational Relationships in Electroencephalograms. In *Advances in Neural Information Processing Systems*, pp. 5377–5386, 2017.
- Weaver, V. M. and McKee, S. A. Can hardware performance counters be trusted? In *2008 IEEE International Symposium on Workload Characterization*, pp. 141–150. IEEE, 2008.
- Wu, H., Damos, G., Cadambi, S., and Yalamanchili, S. Kernel Weaver: Automatically Fusing Database Primitives for Efficient GPU Computation. In *2012 45th Annual IEEE/ACM International Symposium on Microarchitecture*, pp. 107–118, Dec 2012.
- Xu, L., Butt, A. R., Lim, S., and Kannan, R. A Heterogeneity-Aware Task Scheduler for Spark. In *Proc. 2018 IEEE International Conference on Cluster Computing (CLUSTER)*, pp. 245–256, Sep. 2018.
- Yang, H., Breslow, A., Mars, J., and Tang, L. Bubble-flux: Precise Online QoS Management for Increased Utilization in Warehouse Scale Computers. In *Proceedings of the 40th Annual International Symposium on Computer Architecture*, ISCA '13, pp. 607–618, 2013.
- Yasin, A. A Top-Down method for performance analysis and counters architecture. In *Proc. 2014 IEEE International Symposium on Performance Analysis of Systems and Software (ISPASS)*, pp. 35–44, March 2014.
- Zaharia, M., Borthakur, D., Sen Sarma, J., Elmeleegy, K., Shenker, S., and Stoica, I. Delay Scheduling: A Simple Technique for Achieving Locality and Fairness in Cluster Scheduling. In *Proceedings of the 5th European Conference on Computer Systems*, pp. 265–278, 2010.
- Zaharia, M., Bolosky, W. J., Curtis, K., Fox, A., Patterson, D., Shenker, S., Stoica, I., Karp, R. M., and Sittler, T. Faster and more accurate sequence alignment with SNAP. *arXiv preprint arXiv:1111.5572*, 2011.
- Zaharia, M., Chowdhury, M., Das, T., Dave, A., Ma, J., McCauley, M., Franklin, M. J., Shenker, S., and Stoica, I. Resilient Distributed Datasets: A Fault-tolerant Abstraction for In-memory Cluster Computing. In *Proceedings of the 9th USENIX Conference on Networked Systems Design and Implementation*, NSDI'12, pp. 15–28, 2012.
- Zhang, Y., Laurenzano, M. A., Mars, J., and Tang, L. SMiTe: Precise QoS Prediction on Real-System SMT Processors to Improve Utilization in Warehouse Scale Computers. In *2014 47th Annual IEEE/ACM International Symposium on Microarchitecture*, pp. 406–418, Dec 2014.
- Zhu, P., Li, X., Poupart, P., and Miao, G. On improving deep reinforcement learning for POMDPs. *arXiv preprint arXiv:1804.06309*, 2018.
- Zhuravlev, S., Blagodurov, S., and Fedorova, A. Addressing Shared Resource Contention in Multicore Processors via Scheduling. *SIGPLAN Not.*, 45(3):129–142, March 2010.
- Zook, J. M., Catoe, D., McDaniel, J., Vang, L., Spies, N., Sidow, A., Weng, Z., Liu, Y., Mason, C. E., Alexander, N., Henaff, E., McIntyre, A. B., Chandramohan, D., Chen, F., Jaeger, E., Moshrefi, A., Pham, K., Stedman, W., Liang, T., Saghbini, M., Dzakula, Z., Hastie, A., Cao, H., Deikus, G., Schadt, E., Sebra, R., Bashir, A., Truty, R. M., Chang, C. C., Gulbahce, N., Zhao, K., Ghosh, S., Hyland, F., Fu, Y., Chaisson, M., Xiao, C., Trow, J., Sherry, S. T., Zaranek, A. W., Ball, M., Bobe, J., Estep, P., Church, G. M., Marks, P., Kyriazopoulou-Panagiotopoulou, S., Zheng, G. X., Schnall-Levin, M., Ordonez, H. S., Muditvarti, P. A., Giorda, K., Sheng, Y., Rypdal, K. B., and Salit, M. Extensive sequencing of seven human genomes to characterize benchmark reference materials. *Scientific Data*, 3:160025, Jun 2016.

Supplementary Material

A. Extended Motivational Example

Current schedulers prioritize the use of simple online heuristics (Grandl et al., 2016b) and coarse-grained resource bucketing (e.g., core counts, free memory) and require user labeling of commonly used system resources (Hindman et al., 2011; Grandl et al., 2016a) to make scheduling decisions. Those approaches are untenable in truly heterogeneous settings as (i) defining such heuristics is difficult over the combinatorial space of application-processor/accelerator configurations; and (ii) user-based resource usage labeling requires in-depth understanding of the underlying system. This paper demonstrates the use of ML to automatically infer such heuristics and their evolution over time as new user workloads and/or new accelerators are added.

A.1. Dealing with Architectural Heterogeneity

We reiterate that state-of-the-art schedulers do not model the emergent heterogeneous compute platforms that are being widely adopted in data centers and hence leave a lot to be desired (as can also be seen in the performance of our baselines). Consider, for example, the execution of the *forward algorithm on PairHMM models* (Banerjee et al., 2017), a computation that is commonly performed in computational genomics workloads. Fig. 11 shows the significant diversity (nearly 100x) in performance of this single workload across CPUs (from Intel and IBM), GPUs (two models of GPUs from NVIDIA) and FPGA implementations. The increasing heterogeneity necessitates rethinking of the design and implementation of future schedulers, as the current approach will require an extraordinary amount of manual tuning and expertise to adapt to the emergent systems. In contrast, the proposed technique eliminates that work and automates the whole process of learning the right granularity of resources and scheduling workloads in cloud-based, dynamic, multi-tenant environments, thereby improving application

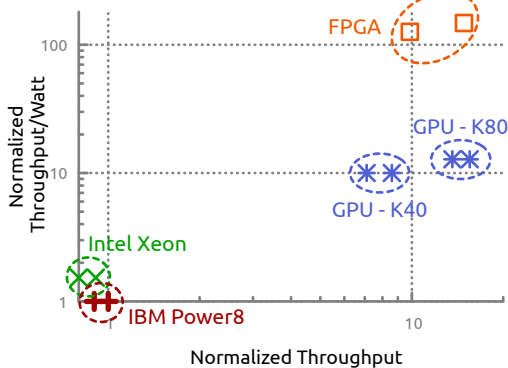


Figure 11. Architectural diversity leading to varied performance for the PairHMM kernel.

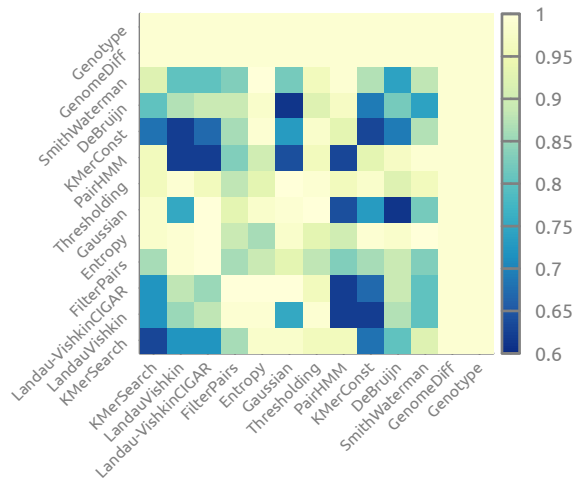


Figure 12. Degradation in runtime of co-located kernels due to shared resource contention.

performance and system utilization, all with minimal human supervision. Prior work uses microarchitectural throughput metrics such as clock cycles per instruction (Giceva et al., 2014; Delimitrou & Kozyrakis, 2013; 2014; Mars et al., 2011; Mars & Tang, 2013) as proxies for processor affinities. In our case, such metrics are not usable because of the wide diversity in processors, i.e., CPU-centric units cannot describe the performance of GPUs/FPGAs.

A.2. Dealing with Resource Granularity

Traditional schedulers use coarse-grained resource bucketing, i.e., they schedule macro-resources like CPU core counts and GBs of memory. That simplifies the design of the scheduling algorithms (both the optimization algorithms and attached heuristics), resulting in an inability to measure low-level sources of resource contention in the system. The contention of such low-level resources is often the cause for performance degradation and variability. Consider, for example, the concurrent execution of several compute kernels (described in Appendix C.2) on co-located hyper-threads (i.e., threads that share resources on a single core) on an Intel CPU. If we abstract the problem at the level of CPU threads and memory allocated, then those kernels should execute in isolation. The normalized runtime variation is illustrated in Fig. 12. We observe a slowdown of as much as 40% (i.e., the co-located runtime is 60% of the isolated runtime) for some combinations of kernels, and almost no slowdown for others. That problem is further exacerbated by the architectural diversity in processors that we described earlier. The proposed technique accounts for such contention by explicitly collecting information on low-level system state by using performance counter measurements, and by estimating resource usage in the system by explicitly encoding

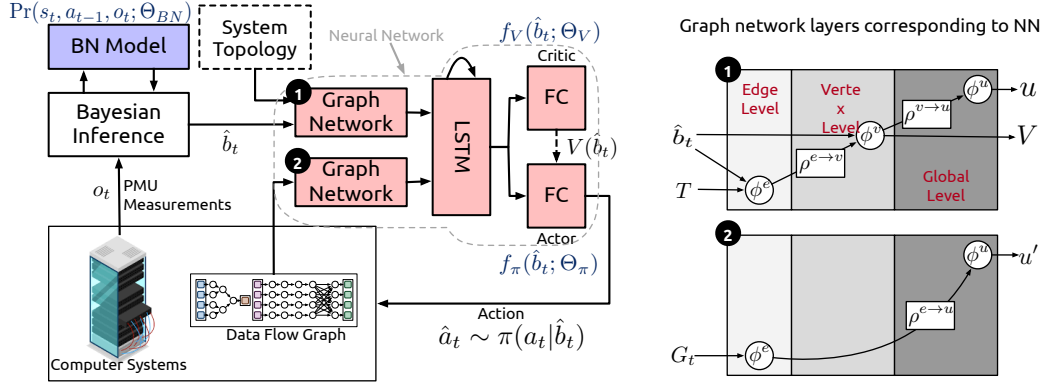


Figure 13. Proposed POMDP model.

the measurements in its POMDP model.

B. Implementation Details

The scheduling framework functions as follows.

1. The scheduler first makes measurements by using the available processor performance counters (e.g., instructions retired, cache misses).
2. When a processor becomes idle (finishes running the current kernel), it invokes the scheduler.
3. The measurements are fed into the scheduler’s BN model as input. Using those measurements, the BN model computes the utilization of different levels of architectural resources in the system (e.g., memory bandwidth utilization, PCIe link utilization). We refer to those utilizations as the *state* of the system.
4. The computed utilization numbers, user programs represented as a DFG, and a system topology graph are fed into an NN. The NN produces a scheduling decision that is actuated in the system. The action space consists of a kernel-processor pair.
5. Finally, the scheduler gets feedback from the system (i.e., the reward) in terms of the time it took for the job to run as a result of its scheduling decision.
6. While in *training mode*, if an incorrect decision is made, Symphony enqueues an update of the policy parameters using back-propagation on the A2C/A3C loss function. An incorrect decision is one where kernel input-output dependencies are not respected, or a kernel-accelerator pair is picked where the accelerator does not provide an implementation of the kernel.

B.1. Graph Network Details

The structure of the graph network used in the proposed model is illustrated in Fig. 13. The numbers of parameters used in the different layers of the graph network are listed in Table 2.

Table 2. Mapping of the graph network layer functions in Fig. 13. We use the notation $FCNN(a, b)$ to denote a 2-hidden fully-connected layers with a and b hidden units, respectively.

Function in GN	Function in 1	Function in 2
ϕ^e	$FCNN(64, 32)$	$FCNN(64, 32)$
ϕ^v	$FCNN(32, 16)$	–
ϕ^u	$FCNN(16, 16)$	$FCNN(32, 16)$
$\rho^{e \rightarrow v}$	$\sum e$	–
$\rho^{v \rightarrow u}$	$\sum v$	–
$\rho^{e \rightarrow u}$	–	$ReLU(e)$

B.2. Hyperparameters

The hyperparameters used to train the proposed POMDP model are listed in Table 3.

B.3. System Measurement Details

Topology Information. Consider the example of standard NUMA based computing system with PCIe based accelerators shown in Fig. 14. The system contains (i) multiple CPUs which have non-uniform access to memory, (ii) several accelerators (including GPUs and FPGAs) each with their own memory, and (iii) a system interconnect which connects all of the components of the system together. Symphony encodes the system topology as a graph $T = (P, N)$ (also shown in Fig. 14). The nodes of the graph P correspond to the processing elements (and attached memory) and memory/system interconnects. Each of these nodes $p \in P$ have an attached resource utilization vector. For example, in an Intel processor, the utilization vector would

Table 3. Hyperparameters used in the model.

Hyperparameter	Value
Learning Rate	0.005
LSTM Unroll Length	20
n_s	20
n_e	2

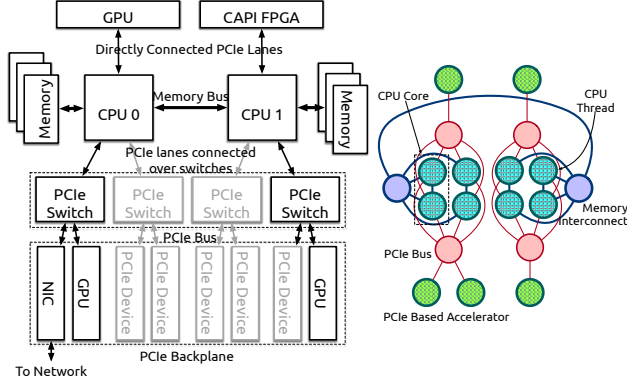


Figure 14. Example of a dual-socket NUMA-based system topology with a PCIe-interconnect and -devices. Figure on the right shows an graph-encoding of the topology.

include utilization like that of micro-op issue ports, floating point unit utilization etc. (Doweck, 2016; Intel Corp., 2014).

The scheduler queries the system topology and builds the topology graph T (which is used as an input to the RL agent) using hwloc (Broquedis et al., 2010). hwloc provides information about CPU cores, caches, NUMA memory nodes, and the PCIe interconnect layout (i.e., connections between the PCIe root complex and PCIe switches), as well as connection information on peripheral accelerators, storage, and network devices in the system. The scheduler does not explicitly model the rack-scale or data center network (unlike some previous approaches, e.g., Isard et al. (2009); Chowdhury et al. (2014)), but the BN and RL model can be extended to do so. Our measurements considers injection bandwidth at the network interface card (NIC) to be a proxy for network performance, i.e., the NIC is modeled as an accelerator that accepts data at $\min(\text{PCIe Bandwidth, Injection Bandwidth})$.

Performance Counter Measurements. Performance counters’ configuration and access instructions require kernel mode privileges, and hence those operations are supported by Linux: system calls to configure and read the performance counter data. Symphony uses a combination of user-space tools, e.g., libPAPI (Terpstra et al., 2010), PMUTools (Kleen, 2010), and perf that wrap around the system call interface to make both system-specific and system-independent measurements.

We configure the performance counters to make system-wide measurements (i.e., for all processes). If the performance counter measurements are configured in that way, it might incur security risks, particularly by opening up side channels through which attackers could infer workload characteristics. However, analysis or mitigation of such risks is not in the scope of this paper and may form the basis of future work.

All kernel executions are non-preemptive in the context

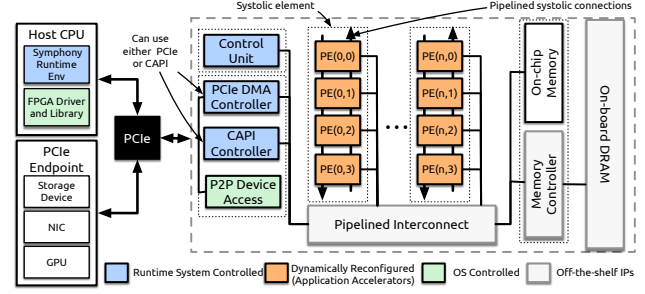


Figure 15. Architecture of the FPGA-based hardware co-processor controlled by Symphony.

of the proposed runtime, however the OS scheduler can preempt CPU threads. Further we prevent the OS scheduler from re-balance tasks/threads once assigned to a particular CPU. This is achieved by explicitly setting affinities of threads to cores (i.e., pinning them).

Performance Penalties. Monitoring of performance counters without having to perform interrupts is almost free. In our implementation, we capture on-core performance counters directly before and after a single kernel invocation. Un-core performance counters are measured periodically (every million dynamic instructions on a core) by using a *performance monitoring interrupt*. On an IBM PowerPC processor, the interrupt handler initiates a DMA transfer of the performance counters to memory (Sudhakar & Srinivasan, 2019), thereby incurring no performance penalty (other than the time to service the interrupt). On Intel processors, the interrupt handler has to explicitly read the performance counter registers and write them to memory. In our tests (on Intel processors), we observed a $\sim 3\%$ performance penalty for applications with interrupts enabled. That corresponds to an execution of a usermode interrupt with an average 900-ns latency.

Distributed Execution. In our evaluation we have deployed Symphony in a rack-scale distributed context (over an EDR Infiniband network fabric) as a centralized scheduler controlling all processing resources. Here, all the performance counter measurements are sent over the network to a centralized server that makes scheduling decisions. This approach works well at the scale of a rack, where all resources are essentially one hop away at 0.2- μs latency. Extending Symphony to larger or slower networks might present challenges, where network latency causes stale performance counter data to reach the scheduler. We will address these challenges in future work.

B.4. Dynamically Reconfigurable FPGA Accelerator

Our implementation and evaluation of Symphony uses a custom FPGA accelerator (see Fig. 15). Due to space limitations, here we briefly describe the features of the accelerator.

- *Processing Elements (PEs).* The co-processor is opti-

Table 4. Hardware specifications of test cluster.

Name	#	Specifications
M1	2	CPU IBM Power8 (SMT 8); 870 GB RAM; GPU NVIDIA K80; FPGA Alpha Data 7V3
M2	4	CPU IBM Power8 (SMT 4); 512 GB RAM; GPU NVIDIA K40; FPGA Nallatech 385
N	1	Mellanox FDR Infiniband

mized to execute the computational kernels as a single instruction of the application. Sets of four neighboring PEs are directly connected as a systolic element, thereby enabling high bandwidth data transfer in between PEs and forming the quantum of reconfiguration.

- *Host-FPGA Communication.* The board interfaces with the host CPU over PCIe and can be configured to communicate with the host processor over this interface in one of two ways: (i) using direct memory access (DMA) to the hosts memory over the PCIe bus, or (ii) using IBM’s coherent accelerator processor interface (CAPI) (Stuecheli et al., 2015).
- *Dynamic Reconfiguration.* The configuration of the accelerator (i.e., which kernels PEs are available at any time) is controlled by Symphony. Symphony treats the reconfiguration of the accelerator as a kernel that has to be dispatched to the FPGA. The state of the accelerator is fed into Symphony along with the system topology T .
- *Launching Kernels.* Remember CPU executors (i.e., threads which are given tasks to execute) are pinned or bound to underlying hardware SMT thread. Accelerators however require the CPUs to initiate their execution. As a result, each accelerator in the system is assigned a proxy executor thread that orchestrates (i.e., launches, polls for completion etc.) its execution. These executors are responsible for managing their own queues for maintaining tasks that are “waiting” for execution.

C. Evaluation Environment

C.1. Evaluation System

All evaluation experiments are performed on an 11 node rack-scale test-bed of IBM Power8 CPUs, NVIDIA K40 and K80 GPUs, as well as FPGAs (listed in Table 4). All the machines in the cluster are connected using a single switch EDR Infiniband network.

C.2. Evaluation Workloads

We illustrated the generality of the proposed approach on a variety of real-world workloads (listed in Table 5) that used CPUs, GPUs, and FPGAs:

1. *variant-calling and genotyping analysis* (Van der Auwera et al., 2013) on human genome datasets appropriate for clinical use (consisting of Align, IR, and HC in Table 5),
2. *epilepsy detection and localization* (Varatharajah et al., 2017) on intra-cranial electroencephalography data; and
3. *online security analytics* (Cao et al., 2015) on network- and host-level intrusion detection system event-streams.

For the variant-calling and genotyping workload we use the NA12878 genome sample from the GIAB consortium (Zook et al., 2016) for all our experiments as it is representative of human clinical datasets. For the EEG and AT workloads, we use the same datasets as discussed in the original papers.

Table 5. Enumeration of workloads used to evaluation.

Application	Processors			Implementations
	CPU	GPU	FPGA	
Alignment (<i>Align</i>)	✓	✓	✓	(Li & Durbin, 2009; 2010; Langmead et al., 2009; Zaharia et al., 2011; Banerjee et al., 2019a; 2016),
Indel Realignment (<i>IR</i>)	✓	✗	✗	(McKenna et al., 2010; Nothaft et al., 2015)
Variant Calling (<i>HC</i>)	✓	✓	✓	(Li et al., 2009; McKenna et al., 2010; Nothaft, 2015; Rimmer et al., 2014; Banerjee et al., 2017)
EEG-Graph (<i>EEG</i>)	✓	✓	✓	(Varatharajah et al., 2017; Banerjee et al., 2019b)
AttackTagger (<i>AT</i>)	✓	✓	✓	(Cao et al., 2015; Banerjee et al., 2019b)